CRYSTAL GROWTH & DESIGN

Communication

pubs.acs.org/crystal

Wetting of Ga on SiO_x and Its Impact on GaAs Nanowire Growth

Federico Matteini,[†] Gözde Tütüncüoglu,[†] Heidi Potts,[†] Fauzia Jabeen,[‡] and Anna Fontcuberta i Morral*[,†]

[†]Laboratoire des Matériaux Semiconducteurs and [‡]Laboratoire d' Optoélectronique Quantique, École Polytechnique Fédérale de Lausanne, 1015 Lausanne, Switzerland

Supporting Information

ABSTRACT: Ga-assisted growth of GaAs nanowires on silicon provides a path for integrating high-purity III−Vs on silicon. The nature of the oxide on the silicon surface has been shown to impact the overall possibility of nanowire growth and their orientation with the substrate. In this work, we show that not only the exact thickness, but also the nature of the native oxide determines the feasibility of nanowire growth. During the course of formation of the native oxide, the surface energy varies and results in a different contact angle of Ga droplets. We find that, only for a contact angle around 90° (i.e., oxide thickness ∼0.9 nm), nanowires grow perpendicularly to the silicon substrate. This native oxide engineering is the first step toward controlling the self-assembly process, determining mainly the nanowire density and orientation.

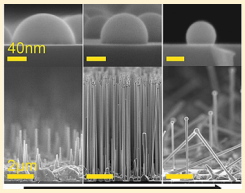

Semiconductor nanowires bring a wide range of new concepts for next generation optoelectronic and electronic technologies, as well as new platforms for fundamental science.[1−7] Among all the III/V semiconductors that can be used to form these structures, GaAs and InP are among the most promising for photovoltaic applications due to its ideal bandgap.[8,9] However, GaAs is technologically more relevant due to the wider availability of Ga in the Earth's crust with respect to In. Moreover, GaAs nanowire solar cells can also be obtained on silicon platforms, creating the possibility of a double junction.[10] Still (to date), no device with GaAs nanowires is commercially available. For several reasons, the fabrication challenges could be invoked. The most common mechanism used for the formation of nanowires is the so-called vapor liquid solid (VLS).[11] This technique requires a liquid droplet, often called a catalyst, which decomposes and/or preferentially gathers the growth precursors in vapor phase. Upon supersaturation of the liquid, a solid phase precipitates underneath. Au is the most widely used metal to induce VLS. Several studies show that Au atoms can get incorporated in the body of the nanowire and on the silicon substrate.[12−15] To circumvent the use of gold for nanowire growth, several groups have studied self-catalyzed or catalyst-free growth of nanowires on silicon.[16−23] Detailed understanding of this particular growth mechanism has led to a better control of the nanowire morphology and crystal phase.[18,19,24−30] However, to date, full control over nanowire orientation was observed to be dependent on the wafer batch.[31,32] Most studies focus on the comprehension of the growth at the steady state. To the best of our knowledge, very little work has targeted the understanding of the initial steps of growth. This phase is key in the heterogeneous integration of III−Vs on silicon as it influences all the subsequent stages.[19,33] In the present work we investigate the influence of the surface properties of the native silicon oxide on the initial growth stages of self-catalyzed GaAs nanowires obtained by molecular beam epitaxy (MBE). In particular, we show how the native oxide thickness is strictly related to nanowire orientation with respect to the substrate, and which conditions are needed to achieve only vertical growth.

We start by describing the preparation of the substrates. We use 2 in. Si(111) wafers with a nominal resistivity of 10−20·Ω*cm. The doping of the wafer only determines the kinetics of oxide formation. All wafers were initially immersed in a BHF solution (7:1) for 2 min to remove the native oxide, and subsequently exposed to air in a controlled cleanroom environment (21 ± 0.5 °C, 44% humidity) for a determined time. The native oxide thickness was monitored with a Sopra GES 5E spectroscopic ellipsometer. The thickness obtained by ellipsometry has been confirmed by AFM measurements on oxide steps (see SI). The temporal evolution of the native oxide thickness after the HF etching is shown in Figure 1a. The native oxide regrows at the fastest pace after the immediate removal of the native oxide. Within a week, a thickness of ∼0.8 nm is achieved. After this initial period, the oxidation slows down, reaching a final thickness of ∼1.5 nm in a much longer time frame, e.g., 20 weeks, as observed earlier in previous studies.[34,35]

After preparing the substrates with a native oxide of particular thickness, we introduce them in the ultra-high-vacuum environment of our MBE machine (DCA P600). For the sake of removing any remnant water or organic residues from the surface, the substrates undergo several degassing steps. First, a halogen lamp degasses the substrates and substrate holder at ∼150 °C for 2 h in the MBE load-lock (between 10^{-6} and 10^{-8} Torr). After this, the wafers are heated to ∼500 °C in a separate chamber for 2 h at a pressure ∼10^{-10} Torr. A third and last degassing is performed in the growth chamber directly prior to growth at 750 °C for 20 min.

We compare the growth for different thicknesses of the native oxide (from 0 to 1.5 nm). All growth was performed

Received: March 18, 2015
Revised: May 20, 2015
Published: May 21, 2015

DOI: 10.1021/acs.cgd.5b00374
Cryst. Growth Des. 2015, 15, 3105−3109

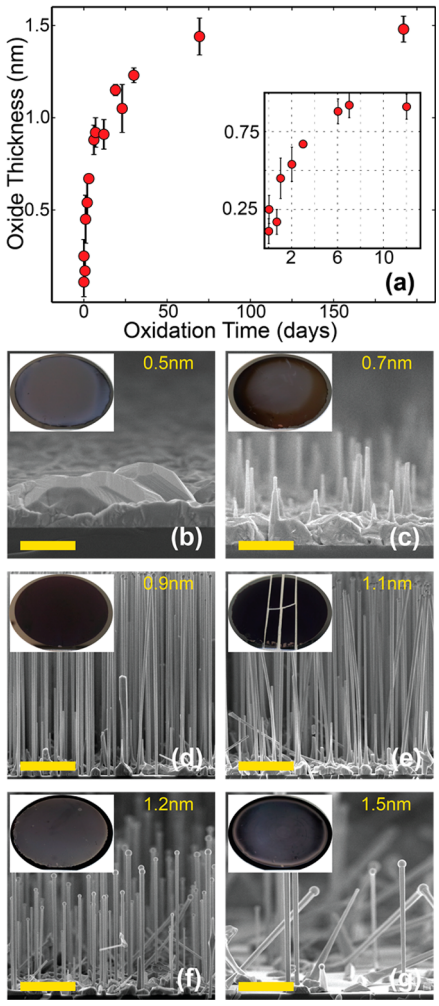

Figure 1. (a) Evolution of the thickness of native oxide as a function of time, as measured by ellipsometry. The inset shows the growth of the native oxide thickness in a smaller time frame (up to 12 days). (b–g) Optical images of the wafers after GaAs growth on the 2 in. wafers and corresponding SEM micrographs of the growth performed at the oxide thicknesses of 0.5, 0.7, 0.9, 1.1, 1.2, and 1.5 nm, respectively. The scale bar is 1 μm.

under identical conditions, which corresponds to a standard for Ga-assisted growth of GaAs nanowires: 640 °C substrate temperature, a Ga rate of 1.1 Å/s, As flux of 2.5×10^{-6} Torr, and growth time of 1 h.[32] Optical and scanning electron microscopy images (SEM) of the samples after growth are shown in Figure 1b–g. For thicknesses of ∼0.5 nm or less, no nanowires are observed. In this case, only polycrystalline GaAs growth is observed (see Figure 1b). At an oxide thickness of around ∼0.7 nm, elongated vertical structures start to form on the polycrystalline layer. Interestingly, these short nanowires mostly exhibit a perpendicular relation with the substrate surface and do not exhibit a droplet at their tip (see Figure 1c). This represents the transition from 2D growth toward Ga-assisted GaAs nanowire growth, which is achieved for oxides thicker than ∼0.9 nm (see Figure 1d). As can be observed in the optical micrographs, the appearance of the samples is homogeneous over the 2 in. wafer. SEM investigations confirm that this is the case. For a native oxide thickness of 0.9 nm only vertical nanowires are observed. Growths performed at oxide thicknesses of 1.1, 1.2, and 1.5 nm present nanowires across the full 2″ wafer (see, respectively, Figure 1d–f). By increasing the native oxide thickness, we observe a progressive increase of nonvertical orientations, a broadening of length and diameter distributions, as well as a decrease of nanowire density.

A more detailed analysis of the nanowire morphology is given in Figure 2: in (a–d) tilted views of the nanowire forests

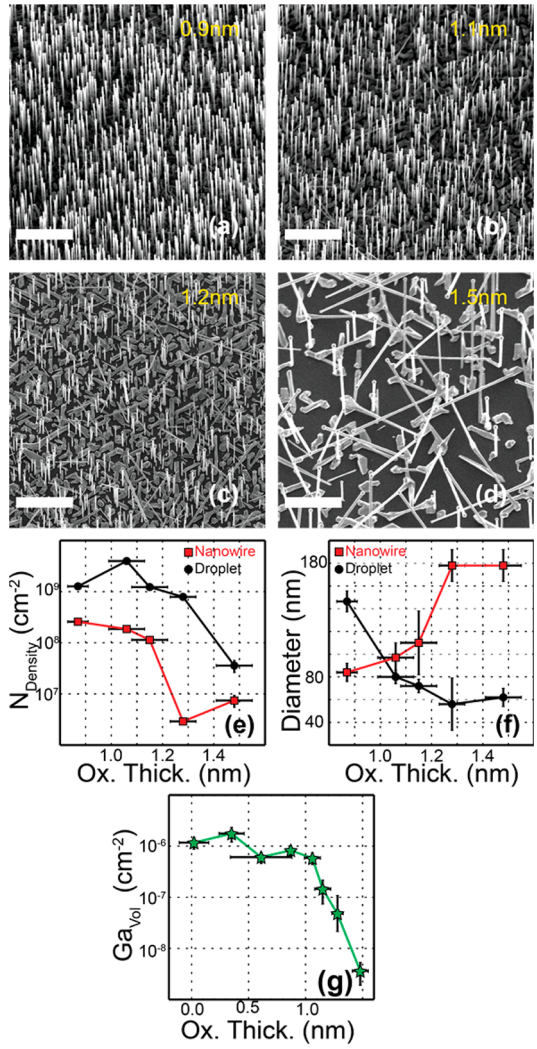

Figure 2. (a–d) SEM micrographs of GaAs nanowires grown on, respectively, 0.9, 1.1, 1.2, and 1.5 nm native oxide on Si (111) substrates. The scalebar is 3 μm. In (e) the density change of nanowires and Ga droplets at increasing oxide thickness is quantified: in both cases the decrease in density is 2 orders of magnitude, although the droplet density is 1 order of magnitude higher: nanowire density goes from $(2.6 \pm 0.03) \times 10^8$ to $(4.7 \pm 0.4) \times 10^6$ cm^{-2}, whereas droplet density goes from $(4.0 \pm 0.23) \times 10^9$ to $(3.6 \pm 1.0) \times 10^7$ cm^{-2}. In (f) the diameter evolution for nanowires and droplets at different oxide thicknesses is represented. Nanowire diameter rises by ∼100 nm (from 84 ± 8 to 186 ± 12 nm), at increasing oxide thickness, whereas the droplet diameter diminishes (from 145 ± 9 to 62 ± 8 nm). In (g) the volume of Ga on the Si substrates after deposition as a function of oxide thickness is represented.

grown on, respectively, 0.9, 1.1, 1.2, and 1.5 nm oxide thickness show a clear decrease in nanowire density and an increase of tilted wires for thicker oxides. The droplets will be discussed in the next paragraph. Quantitatively we observe that the nanowire density drops by 2 orders of magnitude (from 2.6×10^8 to 4.7×10^6cm^{-2}), while the nanowire diameter increases from 90 to 180 nm, as the oxide thickness increases from 0.9 to

DOI: 10.1021/acs.cgd.5b00374
Cryst. Growth Des. 2015, 15, 3105–3109

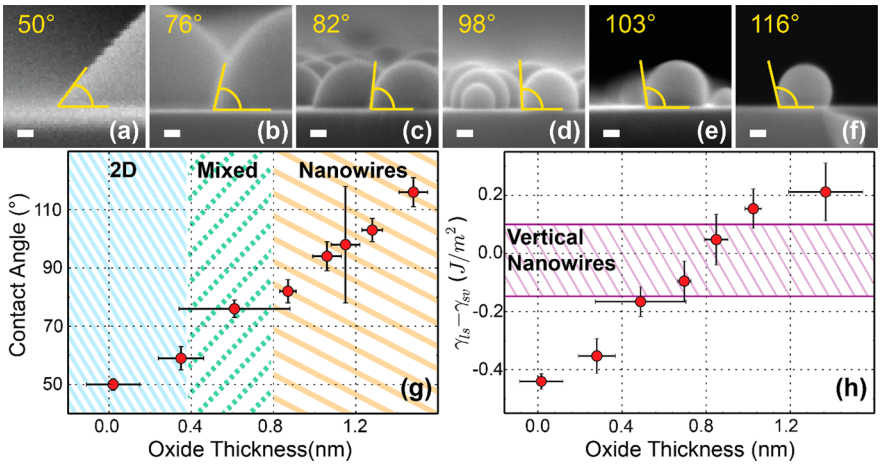

Figure 3. SEM micrographs of the wetting of the Ga droplets formed by Ga deposition at 640 °C for 5 min on oxide thicknesses of 0.1 (a), 0.6 (b), 0.9 (c), 1.1 (d), 1.3 (e), and 1.5 nm (f). The scale bar is 20 nm. In (g) the increase of the contact angle at increased oxide thicknesses is represented. The progress of the contact angle is correlated to the evolution from 2D growth, to mixed 2D-elongated structures without droplets, to nanowire growth. In (h) the surface energy of the different native oxide thicknesses calculated by Young's equation is shown. The range of surface energy at which only vertical nanowire growth was achieved is marked in purple.

1.5 nm. Nanowire populations of >100 were considered for the statistical study.

In order to explain our observations we looked at the initial stage of growth, namely, the formation of the Ga droplets. For this, we deposited Ga for 5 min at the growth temperature. Immediately after the deposition the substrate was cooled down to room temperature for observation. Representative SEM images of the sample surface are shown in the SI. The Ga droplet density and size vary dramatically as a function of the thickness of the native oxide. At ∼0.1 nm of oxide thickness, droplets of diameter above 2 μm are found, while at increasing oxide thicknesses up to 1.5 nm, the droplet diameter progressively shrinks, down to ∼60 nm (see SI).

In Figure 2e,f, the density and diameter of the Ga droplets are compared to the diameter and density of nanowires for oxide thicknesses above 0.8 nm. Ga droplet and nanowire density follow a similar trend. They decrease slightly for oxide thicknesses between 0.8 and 1.1 nm to strongly decrease at higher thickness. Still, there is an order of magnitude difference between the droplet and nanowire density. Unexpectedly, nanowire and droplet diameters evolve in opposite directions: nanowire diameter increases at raising oxide thickness, whereas droplet diameter obtained at a fixed time shrinks. To better understand these counterintuitive results we measured the time required for nanowire growth to start, for different oxide thicknesses. For the sake of simplicity, we will call this time the "incubation time". We monitored the substrate surface by reflection high energy electron diffraction (RHEED) and measured the time lapse until the diffraction peaks of crystalline GaAs nanowires appeared. For oxide thicknesses of 0.9 nm the incubation time was below 10 s, whereas at 1.3 nm it increased up to ∼5 min (see SI). The fact that nanowires start to grow at an earlier time for thinner oxides could explain the smaller nanowire diameter (∼80 nm) compared to the larger nanowire droplet (∼150 nm) achieved with 5 min deposition. The difference in nanowire and Ga droplet diameter for thicker oxides is more difficult to explain, as the incubation time is close to the 5 min of deposition. In this case, the axial growth and nanowire density decrease, which favors the size increase of the Ga droplet during axial growth and thereby the nanowire diameter (further details in SI).

Figure 2g shows the evolution of the amount of Ga found on the surface as a function of the native oxide thickness, calculated by adding the average volume of the droplet times their areal density. The amount of Ga remains constant within the error bar to an oxide thickness of ∼1.0 nm. For thicker oxides it is strongly reduced. This hints at a lower sticking coefficient of the Ga for thicker oxide at the growth temperature. It also indicates a change in the nature of the oxide.[36,37]

In order to further illustrate the change in the nature of the native oxide and to relate it to what one generally observes in nanowire growth,[32] we look at the contact angle of the Ga droplets, β (Figure 3). By progressively increasing the native oxide thickness (0.4, 0.6, 0.9, 1.1, 1.2, and 1.5 nm) the contact angle increases from 50° up to ∼120° (see, respectively, Figure 3a–f). A summary of the contact angle as a function of the oxide thickness is reported in Figure 3g. Interestingly, nanowires form for $\beta > 80°$. The change in contact angle can also be related to the variation of the oxide surface energy through Young's equation:

$$\gamma_{sl} - \gamma_{sv} = \gamma_{lv}\cos(\beta)$$

where γ_{sl} is the liquid–solid surface energy, γ_{sv} is the solid–vapor surface energy, and γ_{lv} is the liquid–vapor surface energy. The latter was calculated by the empirical relation of Hardy.[38] The evolution of the term $\gamma_{sl} - \gamma_{sv}$ is illustrated in Figure 3h: it is negative for an oxide-free silicon surface, therefore energetically favoring the liquid/solid interface formation. The increase in surface thickness leads to an increase of the term $\gamma_{sl} - \gamma_{sv}$. At around 1 nm of oxide thickness $\gamma_{sl} - \gamma_{sv}$ becomes zero (see Figure 3d). From this critical value on, the formation of liquid–solid interface is not favorable, consistent with the high contact angle (>90°). The progressive change in contact angle should be explained by the gradient in the chemical composition of the native oxide. At the Si/SiO_x interface the oxide is silicon-rich. When the distance to the interface (and thickness) is increased, the oxygen content progressively increases. For thick enough layers, typically obtained by thermal oxidation, the composition reaches the stoichiometric composition SiO_2 at ∼1.3 nm off the Si interface.[39−42] Such a variation in chemical composition necessarily results in a change of surface energy.[16,40,42−49]

DOI: 10.1021/acs.cgd.5b00374
Cryst. Growth Des. 2015, 15, 3105−3109

It is worth noting that a contact angle β between 50°and 70° is related to 2D growth. Instead, when the contact angle is larger than 80° nanowire growth becomes viable. Only for contact angles around 90° are a majority of vertical nanowires obtained. Higher contact angles favor the formation of tilted nanowires. This suggests that the initial wetting characteristics of the Ga droplet determine whether or not nanowires are formed, as well as their orientation with respect to the substrate. In principle, the change in nanowire orientation can be due to the following factors: (i) a change in polarity of the first layer nucleating on the silicon substrate or (ii) the existence of three-dimensional multiple twinning.[24] To understand which of the factors is more determining, we measured the tilting angles of the nanowires grown on thicker oxides (1.3 and 1.5 nm). If a change in polarity would be at the origin of the tilted angles, only nanowires with orientations of 19° and 90° would appear. Instead, we observe a wide range of tilting angles consistent with 19°, 34°, 41°, 58°, and 68°. This suggests that (ii) is triggering the formation of multiple orientations. Further work is needed to understand whether the surface energy or thickness of the oxide favors the three-dimensional multiple twinning. One should also consider that the change in surface energy at different oxide thicknesses might influences the Ga diffusion rate, leading to potentially different growth kinetics (e.g., formation of larger Ga droplets). Finally, detailed work on the role of the interface energy between GaAs and the oxide in the initial stage of growth should be performed in the future. For example, one could determine the shape and localization of the initial nuclei as a function of the oxide thickness. One would gain deeper insight into the origin of three-dimensional twinning for thicker layers.

In conclusion, with the present work we have demonstrated the key role of the nature of the native oxide in the Ga-assisted growth process of GaAs nanowires. We have shown that a change in the native oxide thickness is accompanied by a variation of surface energy. This determines the contact angle of Ga droplets on the surface and the capability of forming nanowires as well as their orientation. We find that a contact angle of 90° is the most suitable for obtaining vertical nanowire growth. This work opens new possibilities in nanowire growth in terms of control and reproducibility, also being a step forward toward a realistic integration of compound semiconductor nanowires on the Si platform.

■ ASSOCIATED CONTENT

Supporting Information

Additional characterization. The Supporting Information is available free of charge on the ACS Publications website at DOI: 10.1021/acs.cgd.5b00374.

■ AUTHOR INFORMATION

Corresponding Author

*E-mail: anna.fontcuberta-morral@epfl.ch.

Author Contributions

The manuscript was written through contributions of all authors. All authors have given approval to the final version of the manuscript.

Notes

The authors declare no competing financial interest.

■ ACKNOWLEDGMENTS

The authors thank Eleonora Russo-Averchi, Esther Alarcon-Llado, and Yannik Fontana for the insightful discussions, CIME for the availability of the microscope and funding through Eranet Rus "Incosin", the Nano Tera project "Synergy", SNF through project no 143908 and the ITN Nanoembrace. F. Jabeen thanks ERC project "polaritronics" for funding.

■ REFERENCES

(1) Day, A. W.; Thelander, C.; Lind, E.; Dick, K. A.; Borg, B. M.; Borgstrom, M.; Nilsson, P.; Wernersson, L. E. High-Performance InAs Nanowire MOSFETs. *IEEE Electron Device Lett.* **2012**, *33*, 791.

(2) McAlpine, M. C.; Friedman, R. S.; Jin, S.; Lin, K.-h.; Wang, W. U.; Lieber, C. M. High-performance nanowire electronics and photonics on glass and plastic substrates. *Nano Lett.* **2003**, *3*, 1531.

(3) Tian; Zheng, X.; Kempa, T. J.; Fang, Y.; Yu, N.; Yu, G.; Huang, J.; Liber, C. M. Coaxial silicon nanowires as solar cells and nanoelectronic power sources. *Nature* **2008**, *449*, 885.

(4) Qian, F.; Li, Y.; Gradečak, S.; Park, H.-G.; Dong, Y.; Ding, Y.; Wang, Z. L.; Lieber, C. M. Multi-quantum-well nanowire heterostructures for wavelength-controlled lasers. *Nat. Mater.* **2008**, *7*, 701.

(5) Colombo, C.; Heiss, M.; Grätzel, M.; Fontcuberta i Morral, A. Gallium arsenide p-i-n radial structures for photovoltaic applications. *Appl. Phys. Lett.* **2009**, 173108.

(6) Krogstrup, P.; Jørgensen, H. I.; Heiss, M.; Demichel, O.; Holm, J. V.; Aagesen, M.; Nygard, J.; Fontcuberta i Morral, A. Single-nanowire solar cells beyond the Shockley-Queisser limit. *Nat. Photonics* **2013**, *7*, 306−310.

(7) Mourik, V.; Zuo, K.; Frolov, S. M.; Plissard, S. R.; Bakkers, E. P. A. M.; Kouwenhoven, L. P. Signatures of Majorana fermions in hybrid superconductor-semiconductor nanowire devices. *Science* **2012**, *336*, 1003.

(8) Shockley, W.; Queisser, H. J. Detailed balance limit of efficiency of pn junction solar cells. *J. Appl. Phys.* **1961**, *32*, 510.

(9) Wallentin, J.; Anttu; Asoli, D.; Huffman, M.; Åberg, I.; Magnusson, M. H.; Siefer, G.; Fuss-Kailuweit, P.; Dimroth, F.; Witzigmann, B.; Xu, H. Q.; Samuelson, l.; Deppert, K.; Borgström, M. T. InP nanowire array solar cells achieving 13.8% efficiency by exceeding the ray optics limit. *Science* **2013**, *339*, 1057.

(10) Kandala, A.; Betti, T.; Fontcuberta i Morral, A. General theoretical considerations on nanowire solar cell designs. *Phys. Status Solidi A* **2009**, *1*, 173.

(11) Wagner, S.; Ellis, W. C. Vapor-Liquid-Solid mechanism of single crystal growth. *Appl. Phys. Lett.* **1964**, *4*, 89.

(12) Hemesath, E. R.; Schreiber, D. K.; Gulsoy, E. B.; Kisielowski, C. F.; Petford-Long, A. K.; Voorhees, P. W.; Lauhon, L. J. Catalyst incorporation at defects during nanowire growth. *Nano Lett.* **2012**, *12*, 167.

(13) Breuer, S.; Pfüller, C.; Flissikowski, T.; Brandt, O.; Grahn, H. T.; Geelhar, L.; Riechert, H. Suitability of Au- and self-assisted GaAs nanowires for optoelectronic applications. *Nano Lett.* **2011**, *11*, 1276.

(14) Sze, S. M. *Phys. Semicond. Devices*; Wiley-Interscience: New York, 1981.

(15) Slezák, J.; Ondřejček, M.; Chvoj, Z.; Cháb, V.; Conrad, H.; Heun, S.; Schmidt, T.; Ressel, B.; Prince, K. C. Surface diffusion of Au on Si(111): A microscopic study. *Phys. Rev. B* **2000**, *61*, 16121.

(16) Colombo, C.; Spirkoska, D.; Frimmer, M.; Abstreiter, G.; Fontcuberta i Morral, A. Ga-assisted catalyst free growth mechanism of GaAs nanowires by molecular beam epitaxy. *Phys. Rev. B* **2008**, *77*, 155326.

(17) Paek, J. H.; Nishiwaki, T.; Yamaguchi, M.; Sawaki, N. Catalyst free MBE-VLS growth of GaAs nanowires on (111)Si substrate. *Phys. Status Solidi C* **2009**, *6*, 1436.

(18) Krogstrup, P.; Popovitz-Biro, R.; Johnson, E.; Madsen, M. H.; Nygard, J.; Shtrikman, H. Structural phase control in self-catalyzed growth of GaAs nanowires on Silicon (111). *Nano Lett.* **2010**, *10*, 4475.

DOI: 10.1021/acs.cgd.5b00374
Cryst. Growth Des. 2015, 15, 3105−3109

(19) Mandl, B.; Stangl, J.; Hilner, E.; Zakharov, A. A.; Hillerich, K.; Dey, A. W.; Samuelson, L.; Bauer, G.; Deppert, K.; Mikkelsen, A. Growth mechanism of self-catalyzed group III-V nanowires. *Nano Lett.* **2010**, *10*, 4443.
(20) Plissard, S.; Larrieu, G.; Wallart, X.; Caroff, P. High yield of self-catalyzed GaAs nanowire arrays grown on silicon via gallium droplet positioning. *Nanotechnology* **2011**, *22*, 275602.
(21) Ambrosini, S.; Fanetti, M.; Grillo, V.; Franciosi, A.; Rubini, S. Vapor-liquid-solid and vapor-solid growth of self-catalyzed GaAs nanowires. *AIP Adv.* **2011**, *1*, 042142.
(22) Han, N.; Wang, F.; Hou, J. J.; Yip, S.; Lin, H.; Fang, M.; Xiu, F.; Shi, X.; Hung, T.; Co, J. C. Manipulated growth of GaAs nanowires: controllable crystal quality and growth orientations via a super-saturation-controlled engineering process. *Cryst. Growth Des.* **2012**, *12*, 6243.
(23) Priante, G.; Ambrosini, S.; Dubrovskii, V. G.; Franciosi, A.; Rubini, S. Stopping and resuming at will the growth of GaAs nanowires. *Cryst. Growth Des.* **2013**, *13*, 3976.
(24) Uccelli, E.; Arbiol, J.; Magen, C.; Krogstrup, P.; Russo-Averchi, E.; Heiss, M.; Mugny, G.; Morier-Genoud, F.; Nygard, J.; Morante, R. J.; Fontcuberta i Morral, A. Three-dimensional multiple-order twinning of self-catalyzed GaAs nanowires on Si substrates. *Nano Lett.* **2011**, *11*, 3827.
(25) Glas, F.; Harmand, J.-C.; Patriarche, G. Why does Wurtzite form in nanowires of III-V Zinc Blende semiconductors? *Phys. Rev. Lett.* **2007**, *99*, 146101.
(26) Ramdani, M. R.; Harmand, J.-C.; Glas, F.; Patriarche, G.; Travers, L. Arsenic pathways in self-catalyzed growth of GaAs nanowires. *Cryst. Growth Des.* **2013**, *13*, 91.
(27) Dubrovskii, V. G.; Sibirev, N. V. Growth thermodynamics of nanowires and its application to polytypism of Zinc Blende III-V nanowires. *Phys. Rev. B* **2008**, *77*, 035414.
(28) Krogstrup, P.; Curiotto, S.; Johnson, E.; Aagesen, M.; Nygard, J.; Chatain, D. Impact of the liquid phase shape on the structure of III-V nanowires. *Phys. Rev. Lett.* **2011**, *106*, 125505.
(29) Krogstrup, P.; Jørgensen, H. I.; Johnson, E.; Madsen, M. H.; Sørensen, C. B.; Fontcuberta i Morral, A.; Aagesen, M.; Nygård, J.; Glas, F. Advances in the theory of III−V nanowire growth dynamics. *J. Phys. D: Appl. Phys.* **2013**, *46*, 313001.
(30) Kang, J.-H.; Gao, Q.; Joyce, H. J.; Tan, H. H.; Jagadish; Kim, J.; Guo, Y.; Xu, H.; Zou, J.; Fickenscher, M. A.; Smith, L. M.; Jackson, H. E.; Yarrison-Rice, J. M. Defect-free GaAs/AlGaAs core-shell nanowires on Si substrates. *Cryst. Growth Des.* **2011**, *11*, 3109.
(31) Bastiman, F.; KüPers, H.; Somaschini, C.; Geelhaar, L. Predictive growth of self-assisted GaAs nanowires on Si(111). *EuroMBE Book of Abstracts* **2015**, 101.
(32) Matteini, F.; Tütüncüoğlu, G.; Rüffer, D.; Alarcón-Lladó, E.; Fontcuberta i Morral, A. Ga-assisted growth of GaAs nanowires on silicon, comparison of surface SiOx of different nature. *J. Cryst. Growth* **2014**, *404*, 246.
(33) Fontcuberta i Morral, A.; Colombo, C.; Abstreiter, G.; Arbiol, J.; Morante, J. C. Nucleation mechanism of gallium-assisted molecular beam epitaxy growth of gallium arsenide nanowires. *Appl. Phys. Lett.* **2008**, *92*, 063112.
(34) Raider, S. I.; Flitsch, R.; Palmer, M. J. Oxide growth on etched Silicon in Air at room temperature. *J. Electrochem. Soc.* **1975**, *122*, 413.
(35) Thumser, U.; Beck, P.; Stewart, D. *Stanford Nanofabrication Facility*; 2001; http://snf.stanford.edu/Process/Characterization/SiO2Growth0.pdf.
(36) Shibata, M.; Stoyanov, S. S.; Ichikawa, M. Selective growth of nanometer-scale Ga dots on Si (111) surface windows formed in an ultrathin SiO_2 film. *Phys. Rev. B* **1999**, *59*, 10289.
(37) Nitta, Y.; Shibata, M.; Fujita, K.; Ichikawa, M. Nanometer-scale Si selective growth on Ga-adsorbed voids in ultrathin SiO2 films. *Surf. Sci.* **1999**, *431*, 565.
(38) Hardy, S. C. The surface tension of liquid gallium. *J. Cryst. Growth* **1985**, *71*, 602.
(39) Al-Bayati, A. H.; Orrman-Rossiter, K. G.; van den Berg, J. A.; Armour, D. G. Composition and structure of the native Si oxide by high depth resolution medium energy ion scattering. *Surf. Sci.* **1991**, *241*, 91.
(40) Muller, D. A.; Sorsch, T.; Moccio, S.; Baumann, F. H.; Evans-Lutterodt, K.; Timp, G. The electronic gate structure at the atomic scale of ultrathin gate oxides. *Nature* **1999**, *399*, 758.
(41) Gusev, E. P.; Lu, H. C.; Gustafsson, T.; Garfunkel, E. Growth mechanism of thin silicon oxide films on Si(100) studied by medium energy ion scattering. *Phys. Rev. B* **1995**, *53*, 1759.
(42) Khalilov, U.; Pourtois, G.; Huygh, S.; van Duin, A. C. T.; Neyts, E. C.; Bogaerts, A. New mechanism for oxidation of native silicon oxide. *J. Phys. Chem. C* **2013**, *117*, 9819.
(43) Watanabe, H.; Fujita, S.; Maruno, S.; Fujita, K.; Ichikawa, M. Selective thermal decomposition of ultrathin silicon oxide layers induced by electron-stymulated oxygen desorption. *Appl. Phys. Lett.* **1997**, *71*, 1038.
(44) Chao, S. S.; Tyler, J. E.; Takagi, Y.; Pai, P. G.; Lucovski, G.; Lin, S. Y.; Wong, C. K.; Mantini, M. J. A study of chemical bonding in suboxides of silicon using using Auger electron spectroscopy. *J. Vac. Sci. Technol., A* **1986**, *4*, 1574.
(45) Seah, M. P.; Spencer, S. J.; Bensebaa, F.; Vickridge, I.; Danzebrink, H.; Krumrey, M.; Gross, T.; Oesterle, W.; Wendler, E.; Rheinländer, B.; Azuma, Y.; Kojima, I.; Suzuki, N.; Suzuki, M.; Tanuma, S.; Moon, D. W.; Lee, H. J.; Cho, H. M.; Chen, H. Y.; Wee, A. T. S.; Osipowicz, T.; Pan, J. S.; Jordaan, W. A.; Hauert, R.; Klotz, U.; van der Marel, C.; Verheijen, M.; Tamminga, Y.; Jeynes, C.; Bailey, P.; Biswas, S.; Falke, U.; Nguyen, N. V.; Chandler-Horowitz, D.; Ehrstein, J. R.; Muller, D.; Dura, J. A. Critical review of the current status of thickness measurements for ultrathin SiO2 on Si Part V: Results of a CCQM pilot study. *Surf. Interface Anal.* **2004**, *36*, 1269.
(46) Gusev, E. P.; Lu, H. C.; Gustafsson, T.; Garfunkel, E. Growth mechanism of thin silicon oxide films on Si(100) studied by medium-energy ion scattering. *Phys. Rev. B* **1995**, *52*, 1759.
(47) Ono, H.; Ikarashi, T.; Ando, K.; Kitano, T. Infrared studies of transition layers at SiO_2/Si interface. *J. Appl. Phys.* **1998**, *84*, 6064.
(48) Soria, F. A.; Patrito, E. M.; Paredes-Olivera, P. Oxidation of hydrogenated Si(111) by a radical propagation mechanism. *J. Phys. Chem. C* **2012**, *116*, 24607.
(49) Guichard, A. R.; Barsic, D. N.; Sharma, S.; Kamins, T. I.; Brongersma, M. L. Tunable light emission from quantum-confined excitons in $TiSi_2$-catalyzed silicon nanowires. *Nano Lett.* **2006**, *6*, 2140.

DOI: 10.1021/acs.cgd.5b00374
Cryst. Growth Des. 2015, 15, 3105−3109